AGU ADVANCING EARTH AND SPACE SCIENCES

AGU Advances

RESEARCH ARTICLE
10.1029/2025AV001719

Connecting Warming Patterns of the Paleo-Ocean to Our Future

Xiaoqing Liu[1], **Yi Ge Zhang**[2], **Matthew Huber**[1], **Ping Chang**[3], **and Lei Wang**[1]

[1]Department of Earth, Atmospheric and Planetary Sciences, Purdue University, West Lafayette, IN, USA, [2]State Key Laboratory of Deep Earth Processes and Resources (DEEPER), Guangzhou Institute of Geochemistry, Chinese Academy of Sciences, Guangzhou, China, [3]Department of Oceanography, Texas A&M University, College Station, TX, USA

Peer Review The peer review history for this article is available as a PDF in the Supporting Information.

Key Points:

- A novel regression-based technique is used to establish the spatial pattern of sea surface temperature change over the past 10 million years
- Paleo-ocean warming patterns resemble those from equilibrated simulations under high CO_2 levels but differ from recent warming patterns
- Combining paleo-ocean warming pattern with equilibrated simulations helps predict the future equilibrium pattern of ocean surface warming

Supporting Information:

Supporting Information may be found in the online version of this article.

Correspondence to:

Y. G. Zhang,
zhangyige@gig.ac.cn

Citation:

Liu, X., Zhang, Y. G., Huber, M., Chang, P., & Wang, L. (2025). Connecting warming patterns of the paleo-ocean to our future. *AGU Advances*, *6*, e2025AV001719. https://doi.org/10.1029/2025AV001719

Received 6 MAR 2025
Accepted 21 AUG 2025

Author Contributions:

Conceptualization: Xiaoqing Liu, Yi Ge Zhang, Matthew Huber
Data curation: Xiaoqing Liu
Formal analysis: Xiaoqing Liu
Funding acquisition: Yi Ge Zhang, Matthew Huber
Investigation: Xiaoqing Liu, Yi Ge Zhang, Matthew Huber, Ping Chang
Methodology: Xiaoqing Liu, Yi Ge Zhang, Matthew Huber, Ping Chang, Lei Wang
Project administration: Yi Ge Zhang
Resources: Xiaoqing Liu, Yi Ge Zhang

Abstract The evolution of the spatial pattern of ocean surface warming affects global radiative feedback, yet different climate models provide varying estimates of future patterns. Paleoclimate data, especially from past warm periods, can help constrain future equilibrium warming patterns. By analyzing marine temperature records spanning the past 10 million years with a regression-based technique that removes temporal dimensions, we extract long-term ocean warming patterns and quantify relative sea surface temperature changes across the global ocean. This analysis revealed a distinct pattern of amplified warming that aligns with equilibrated model simulations under high CO_2 conditions, yet differs from the transient warming pattern observed over the past 160 years. This paleodata-model comparison allows us to identify models that better capture fundamental aspects of Earth's warming response, while suggesting how ocean heat uptake and circulation changes modify the development of warming patterns over time. By combining this paleo-ocean warming pattern with equilibrated model simulations, we characterized the likely evolution of global ocean warming as the climate system approaches equilibrium.

Plain Language Summary The uneven ocean surface warming impacts regional climate and climate sensitivity, but the future equilibrium warming pattern predicted by climate models is inconsistent. Paleoclimate data from past warm climates can help constrain this pattern. Using a novel regression-based technique and sea surface temperature (SST) records over the past 10 million years, we established a spatial pattern of SST changes in other regions relative to the Western Pacific Warm Pool. We found a distinct paleo-ocean warming pattern, which resembles some millennial-length model simulations under an abrupt quadrupling of CO_2 concentrations but differs from the warming pattern observed over the recent 160 years. This provides insights into the potential future trajectory of the equilibrium pattern of ocean surface warming.

1. Introduction

The current transient warming during the Common Era is less than the equilibrium warming predicted by Equilibrium Climate Sensitivity (ECS) (Forster et al., 2021), which measures the ultimate global mean surface temperature change per doubling of atmospheric CO_2 levels. This discrepancy is primarily a consequence of slow feedback processes, including the ocean interior's heat capacity, carbon cycle changes, ice-albedo and aerosol feedbacks, and ocean circulation changes (Forster et al., 2021; Gebbie & Huybers, 2019). One process—the dependence of the varying feedbacks on the evolving spatial pattern of ocean surface temperature changes, commonly referred to as the "pattern effect" (Andrews & Webb, 2018; Andrews et al., 2015; Armour et al., 2013; Gregory & Andrews, 2016; Lewis & Mauritsen, 2021)—has gained increasing attention. This effect arises from the uneven sea surface temperature (SST) changes (Andrews et al., 2015) that create distinct ocean warming patterns. These patterns impact atmospheric circulation and stability (Andrews et al., 2015; Dong et al., 2019; Zhou et al., 2017), thus influencing cloud cover, precipitation, and heat transport. This intricate interplay can amplify or dampen warming, influencing climate sensitivity to greenhouse gas emissions. One recent estimate suggests that accounting for the pattern effect cloud increase committed global warming under present-day forcing by up to 1°C (Zhou et al., 2021).

However, the presence of vastly different equilibrium ocean "warming patterns" generated by different climate models (Dong et al., 2020) raises concerns. Moreover, Coupled Model Intercomparison Project Phase 5 (CMIP5) and 6 (CMIP6) simulations show systematic biases in reproducing the observed transient warming patterns (Wills et al., 2022), highlighting the need to evaluate their long-term equilibrium projections against independent

Software: Xiaoqing Liu
Supervision: Yi Ge Zhang, Matthew Huber, Ping Chang
Validation: Xiaoqing Liu, Yi Ge Zhang, Matthew Huber
Visualization: Xiaoqing Liu
Writing – original draft: Xiaoqing Liu, Yi Ge Zhang, Matthew Huber
Writing – review & editing: Xiaoqing Liu, Yi Ge Zhang, Matthew Huber, Ping Chang, Lei Wang

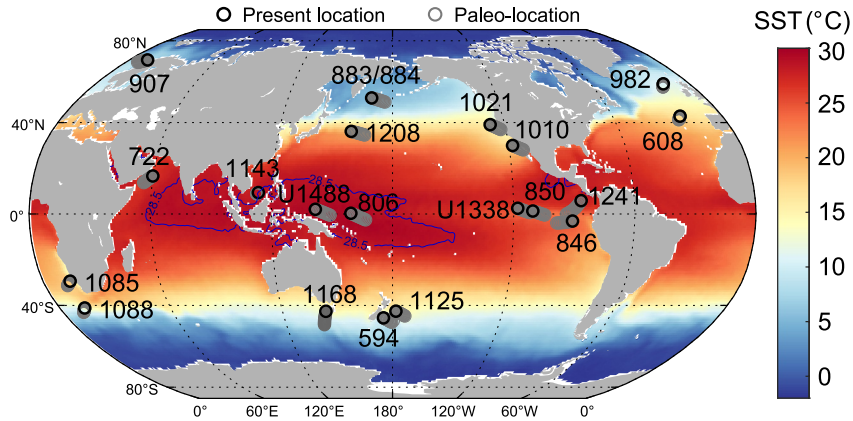

Figure 1. Sites used in this study. The map shows the statistical mean of annual sea surface temperature derived from World Ocean Atlas 2013 (Locarnini et al., 2018). Gray circles at each site represent paleo-locations of the past 10 million years (Myr) at a 1-Myr window. Black circles indicate present locations. Blue contour lines indicate the 28.5°C isotherm that defines the modern Western Pacific Warm Pool.

constraints. These patterns represent the target that the contemporary ocean might evolve toward once radiative equilibrium is achieved. However, the lack of precise knowledge about this "target" introduces major uncertainties in estimating the energy influx due to the pattern effect, posing a key challenge in projecting future warming patterns and their regional climate impacts (Forster et al., 2021).

To constrain these uncertainties in future warming patterns, we can examine periods in Earth's history when the climate system was near equilibrium. Marine temperature records spanning millions of years provide a unique opportunity to observe how warming patterns develop when the ocean has fully adjusted to elevated greenhouse conditions. By comparing these long-term patterns with climate model simulations, we can evaluate which models best capture the fundamental physics of Earth's warming response, improving confidence in projections of future regional climate change.

Extracting warming patterns from individual locations, such as ocean drilling sites, requires careful consideration of how paleoclimate data are compiled and analyzed. Various approaches have been developed, including network-based methods that analyze the spatial co-variability structure of proxy records to reconstruct atmospheric circulation patterns (Franke et al., 2017), and data assimilation techniques that integrate proxy records into climate models to construct comprehensive patterns for specific time periods (Tierney et al., 2020, 2022). Another method normalizes temperature changes from paleoclimate records, enabling direct comparison with modern observations and model projections, independent of temporal variations (Liu et al., 2022). Building upon this latter approach, we establish global ocean warming pattern by analyzing temperature data from sites spanning the past 10 million years (Myr), focusing on relative temperature changes at each site compared to a reference region.

2. Compiling the Global SST Data for the Last 10 Myr

We compiled TEX_{86}, $U^{K'}_{37}$ and Mg/Ca data (Burls et al., 2021a; Lawrence et al., 2021), which were then used to calculate SSTs for the global ocean over the past 10 Myr (Table S1 in Supporting Information S1 and Figure 1). TEX_{86} were converted to SSTs using a Bayesian-based spatially varying regression (BAYSPAR) calibration (Tierney & Tingley, 2014), which considers the spatial variations in TEX_{86}-SST relationships. $U^{K'}_{37}$ were converted to SSTs using a Bayesian B-spline approach (BAYSPLINE) (Tierney & Tingley, 2018), which better handles the nonlinear relationship between $U^{K'}_{37}$ and temperature as the $U^{K'}_{37}$ index approaches 1 and SST closes toward 29°C. This is particularly important for the tropical Sites U1338, 846, 850, 1241, and 722 in our compilation. The Mg/Ca-SST of Site 806 was adjusted using seawater Mg/Ca variations, and carbonate dissolution impact on Mg/Ca thermometry was also considered (Liu et al., 2022).

All SST records were calibrated to the same absolute time frame, GTS 2012 (Gradstein et al., 2012), which is essential for aligning all records before the temporal domain was removed. If major advancements have been made since the original publication of the SST records, we then utilized this new knowledge to enhance the

chronology of these SST time-series. Age estimates of Sites 594 and 1125 were updated using Bacon age-modeling software (Blaauw & Christen, 2011) (https://chrono.qub.ac.uk/blaauw/bacon.html) by combining astronomically-tuned Pliocene age models reported by Caballero-Gill et al. (2019) and previously published age-depth relationships from Herbert et al. (2016). The ages of Site U1338 were updated using a revised bio-magnetostratigraphic age model from Backman et al. (2016).

We focus on the past 10 Myr because this interval represents a period of relatively stable boundary conditions compared to earlier geological periods, with continental configurations broadly similar to modern conditions. While acknowledging that some boundary condition changes occurred during this interval, the overall tectonic stability of this period makes it most appropriate for deriving warming patterns relevant to future climate projections under anthropogenic forcing. We note that our regression-based methodology itself does not require similar boundary conditions—it can extract warming patterns from any time period—but the constraint of boundary condition similarity becomes important when applying these paleoclimate-derived patterns to understand modern and future climate evolution.

However, an important limitation in our model-data comparison is that the SST changes recorded in proxy data over the past 10 Myr were influenced by both CO_2 and non-CO_2 forcings—including changes in paleogeography, solar constant, and aerosols—whereas future climate simulations used in this study are driven exclusively by CO_2 forcing. Different forcing mechanisms can produce distinct spatial patterns of surface temperature change. For example, while increasing atmospheric CO_2 levels generally lead to relatively uniform global warming, paleogeographic changes can have more localized effects. Specifically, the closure of the Bering Strait during the Miocene–Pliocene and the opening of the Canadian Arctic Archipelago during the Miocene are both thought to have warmed the North Atlantic through their impact on ocean circulation (Brierley & Fedorov, 2016; Liu et al., 2024; Otto-Bliesner et al., 2017). The amplification factors estimated from our paleo-data therefore reflect the combined effect of multiple forcings and may not be directly comparable to simulations driven by CO_2 alone. Despite this difference, we believe our comparison provides valuable insights into the spatial characteristics of future equilibrium warming.

3. Establishing the Warming Pattern Over the Last 10 Myr

Building on compiled proxy data for SST reconstructions of the past 10 Myr (Table S1 in Supporting Information S1) around the world's ocean and a study focused on the Western Pacific Warm Pool (WPWP) (Liu et al., 2022), we use a regression-based method to identify the global ocean's warming pattern. Specifically, SST records from non-WPWP regions are regressed against WPWP SST (Figure 2b, Text S1 in Supporting Information S1). The amplification factor relative to the WPWP is defined as the slope of a significant linear regression (p-value < 0.05) between the SST change in non-WPWP regions and the WPWP (Figure 2b), based on York Regression (York et al., 2004), a weighted least squares regression method that accounts for uncertainties in bivariate data, along with the correlation between those uncertainties. This approach enables direct comparisons among paleoclimate, modern-climate, and projected future climate without considering temporal changes.

WPWP—the largest and warmest surface waterbody on Earth—was selected for three primary reasons: (a) the unavailability of direct paleoclimate proxy records of global mean surface temperature over the studied interval, (b) its convective coupling to the upper atmosphere and top-atmosphere energy balance (Fu et al., 1994), which allows its SST to exhibit strong coherence with global mean surface temperature on long timescales (Cleveland Stout et al., 2023), (c) the warming of other regions relative to the WPWP is closely tied to global radiative feedback (Dong et al., 2019; Fueglistaler, 2019), and (d) its geographical location far from the cryosphere and continents, facilitating more statistically robust and interpretable relationships. These physical characteristics make WPWP temperatures particularly relevant for understanding both past and future warming patterns. Our regression-based approach remains valid across a wide range of temperatures, as theoretical and modeling studies (Sud et al., 2008; Williams et al., 2009) have rebutted the concept of a “tropical thermostat,” suggesting no physical basis for a maximum ocean temperature. Indeed, paleo-SST records support this view, showing temperatures exceeding 32°C during the late Miocene (Liu et al., 2022; Zhang et al., 2014), further justifying our use of linear regression against WPWP temperatures across the entire temperature range observed in our data set.

By combining the WPWP SST stack with 17 non-WPWP SST records around the global ocean with necessary temporal resolution and data quality (Table S1 in Supporting Information S1 and Figure 1), we quantified the amplified warming of each non-WPWP site relative to the WPWP, thereby establishing the warming pattern (Text

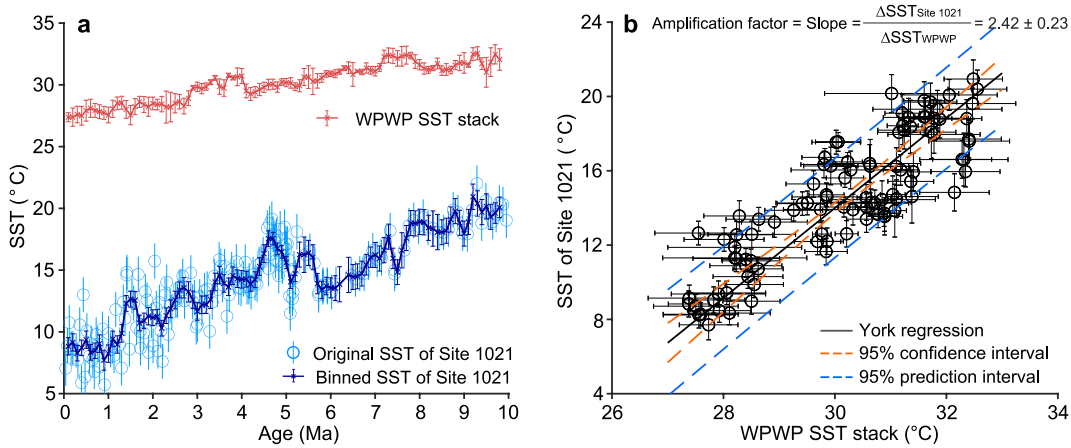

Figure 2. Transforming two sea surface temperature (SST) time series into an amplification factor. (a), Western Pacific Warm Pool (WPWP) SST stack and binned SST of Site 1021. Warm Pool SST stack (red line) was calculated using TEX_{86}-SST from Sites U1488 (Liu et al., 2022), 806 and 1143 (Zhang et al., 2014) and seawater Mg/Ca-adjusted Mg/Ca-SST from Site 806 (Liu et al., 2022). The blue line indicates $U^{K'}_{37}$-derived SSTs of Site 1021 (Herbert et al., 2016), which were binned over 200 kyr, with 50% overlap. (b), Determining the amplification factor for Site 1021 by scatter plotting the SST data of the WPWP and Site 1021 from the same binning intervals, and then performing a linear regression analysis. Error bars indicate 1σ, and the black line represents York Regression. The p-value from this linear regression is less than 0.0001, indicating the linear relationship is statistically significant. The slope, that is, the amplification factor for Site 1021, is 2.42 ± 0.23 (2σ).

S1 in Supporting Information S1). Plate movement's impact on these records seems minor as the SST changes resulting from paleogeographic changes alone fall within the uncertainty range of the reconstructed SST (Text S2 and Figure S1 in Supporting Information S1). The majority of the sites yield amplification factors larger than 1 (Figure 3a), indicating amplified warming of most of the world's ocean relative to the WPWP during Earth's distant history. Also, warming is amplified to a greater extent in high latitudes than in middle latitudes (Figure 3a

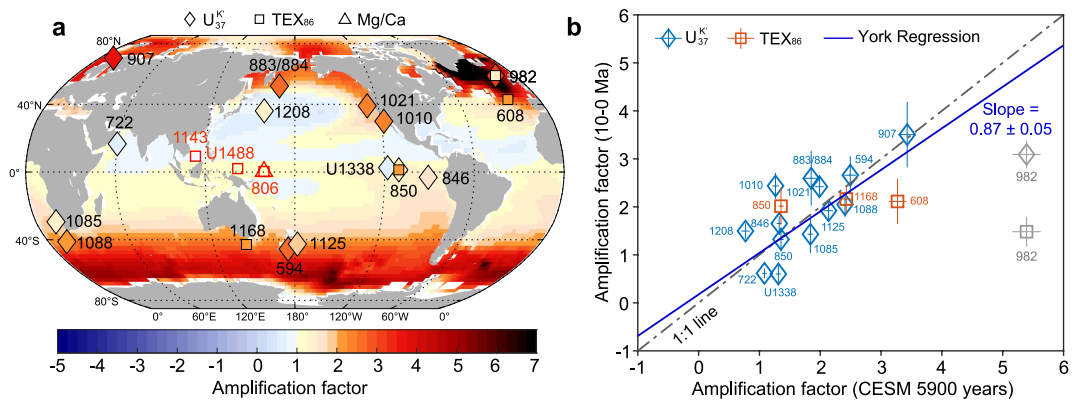

Figure 3. Comparing amplification factors derived from geological data spanning the last 10 million years with those from the CESM simulations. (a) Map shows the model-derived warming patterns of the global ocean. Amplification factors were determined by analyzing model outputs from Community Earth System Model version 1.0.4 (CESM104) run with abrupt atmospheric CO_2 quadrupling above pre-industrial levels integrated over 5,900 years (Rugenstein, Bloch-Johnson, Abe-Ouchi et al., 2020). Only regions where the linear regression between Western Pacific Warm Pool (WPWP) SSTs and local SSTs is significant (p-value < 0.05) were included in our analyses (shown with color). Filled diamonds and squares indicate 10-million-year amplification factors derived from $U^{K'}_{37}$ and TEX_{86}-based SSTs (Text S4 in Supporting Information S1), respectively. Red square and triangle symbols represent the WPWP sites used for producing the WPWP sea surface temperature stack. (b), Comparison between model-derived amplification factors and proxy-derived results. The gray dashed line represents the 1:1 relationship. Error bars indicate two standard errors of the amplification factor. The blue line indicates York Regression (York et al., 2004) with an R-squared of 0.42 (Text S5 in Supporting Information S1) excluding two apparent outliners from Site 982 ($U^{K'}_{37}$ and TEX_{86}), shown as the gray markers. The blue text (0.87 ± 0.05, 1σ) around this line indicates the slope of the linear relationship.

and Figure S2 in Supporting Information S1), providing evidence for the concept of polar or high latitude amplification. This pattern may be enhanced by potential changes in $U^{K'}_{37}$ seasonality during warmer periods, when annual rather than summer production would decrease apparent warming at high-latitude sites (Tierney et al., 2025). While our study reveals key insights into long-term warming patterns, we acknowledge the limited spatial coverage of SST proxy records, particularly in open ocean and high-latitude regions. Future studies can refine our understanding of global warming patterns and climate sensitivity by incorporating new proxy records from underrepresented regions, especially the Southern Ocean.

The amplification factors derived from linear regression for the entire data set (Figure 3) align with those averaged across five different subsets of the data set, which are segmented based on different degrees of the WPWP warming, ranging from 1 to 5°C with a step of 1°C (Text S3 and Figure S3–S5 in Supporting Information S1). This consistency (Figure S5 in Supporting Information S1) indicates that linear regression accurately represents the relationships between non-WPWP and WPWP SSTs across various levels of global warming, presumably capturing an inherent characteristic of the earth's climate system. While linear regression might not encompass all the complexities of the Earth's climate system, it provides a first-order approximation that is useful for understanding the basic physics and patterns of warming.

4. Comparing the Paleo-Warming Pattern With Model Outputs

Applying the regression methods described earlier, we can extend the analysis to both model-predicted future SST changes and recent observed SST change to obtain normalized warming patterns of the global ocean. The model outputs used for comparison in this study are derived from LongRunMIP (Rugenstein, Bloch-Johnson, Abe-Ouchi et al., 2020) simulations under an abrupt quadrupling of atmospheric CO_2 concentration relative to pre-industrial levels (abrupt-4×CO_2). These millennial-length simulations are particularly valuable as they allow us to examine how models project the evolution of warming patterns toward their equilibrium state (Text S6 in Supporting Information S1). Previous research, with a specific focus on the Pacific Ocean, has highlighted the Community Earth System Model (CESM1.0.4) as a noteworthy example, demonstrating its ability to capture high latitude amplifications based on paleo-SST records (Liu et al., 2022). In a similar vein, here we demonstrate that the CESM simulations exhibit a noteworthy level of agreement with the warming patterns established through the analysis of paleo-SST records from 15 sites distributed worldwide (Text S7 in Supporting Information S1, Figure 3).

The amplification factor comparison between the 10-Myr paleoclimate records and the CESM output demonstrates a striking agreement, with the majority of data points closely aligned along the 1:1 line (Figure 3). This agreement is particularly noteworthy given the substantial differences in data acquisition methods and timescales involved, suggesting that CESM captures fundamental aspects of Earth's equilibrium climate response.

Two outliers, specifically Site 982, show a much larger model-derived amplification factor compared to paleo-results (Figure 3b). The model predicts a substantial warming of approximately 6°C for Site 982 (57.516°N, 15.866°W) in the North Atlantic, while the WPWP experiences a much smaller warming of 1.4°C over the simulated 5,900 years. The large warming projected for the North Atlantic by the CESM is probably attributed to a pronounced strengthening of Atlantic meridional overturning circulation (Jansen et al., 2018) and the resulting enhanced northward ocean heat transport. Excluding these two apparent outliners, the York Regression analysis between the modeled and geological data-based amplification factors shows a slope of 0.87 ± 0.05 (p-value < 0.0001, Figure 3b), indicative of an agreement between the two data sets.

In addition to CESM, the LongRunMIP (Rugenstein, Bloch-Johnson, Abe-Ouchi et al., 2020) project includes eight other models that conducted abrupt-4×CO_2 simulations, allowing us to evaluate which models effectively capture the ocean warming pattern. Their warming patterns are computed (Figure 4) and compared with paleo-results (Figures 5a–5h). By analyzing the deviation of the regression line from the 1:1 line (Text S7 in Supporting Information S1, Figures 5a–5h), which represents the proximity of the slope in the York Regression to 1, we find that CCSM3, HadGEM2, and MPIESM11 models demonstrate strong agreement with paleo-results (Figures 5a, 5e, and 5g).

Besides York Regression, we also apply Orthogonal Distance Regression (ODR) (Figure S6 in Supporting Information S1), which accounts for errors of both variables but uses a different minimization approach. ODR yields similar regression slopes to those derived from York Regression, albeit with large uncertainties. To

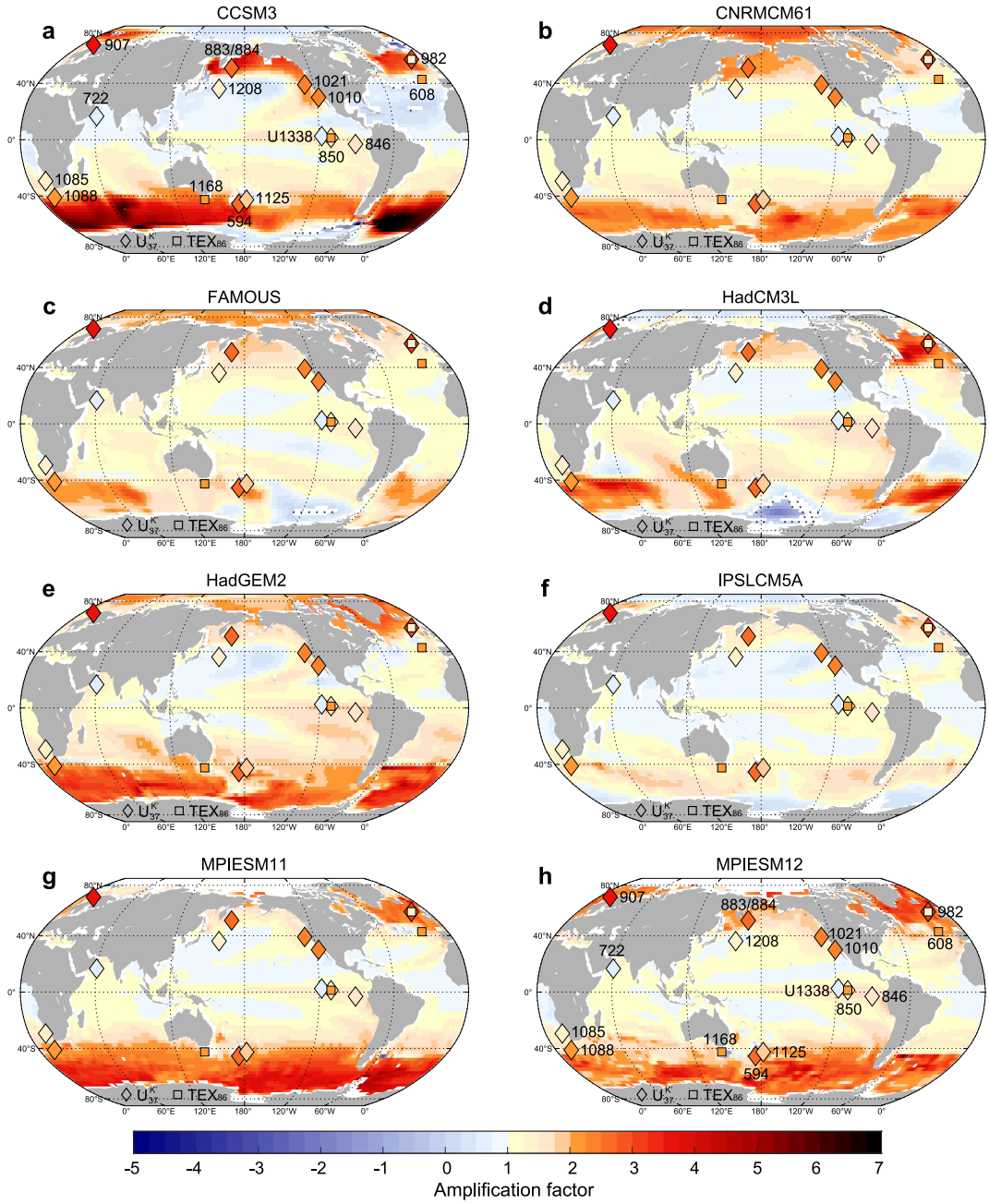

Figure 4. Amplification factors obtained from model simulations of LongRunMIP other than Community Earth System Model. (a–h) Show amplification factors estimated from the sea surface temperature (SST) outputs of CCSM3, CNRMCM61, FAMOUS, HadCM3L, HadGEM2, IPSLCM5A, MPIESM11, and MPIESM12, respectively. Symbols are same as those shown in Figure 3a. Filled diamonds and squares indicate 10-million-year amplification factors derived from $U_{37}^{K'}$-based and TEX_{86}-based SSTs, respectively.

estimate the uncertainty of the regression slope, we apply a bootstrapping approach, resampling our available sites independently with replacement and performing York regression 10,000 times. The resulting slope distributions (Figure S7 in Supporting Information S1) show that the median values align with slopes derived from York regression and ODR using all sites, with uncertainties comparable to those from ODR, particularly in models with lower regression slope uncertainties.

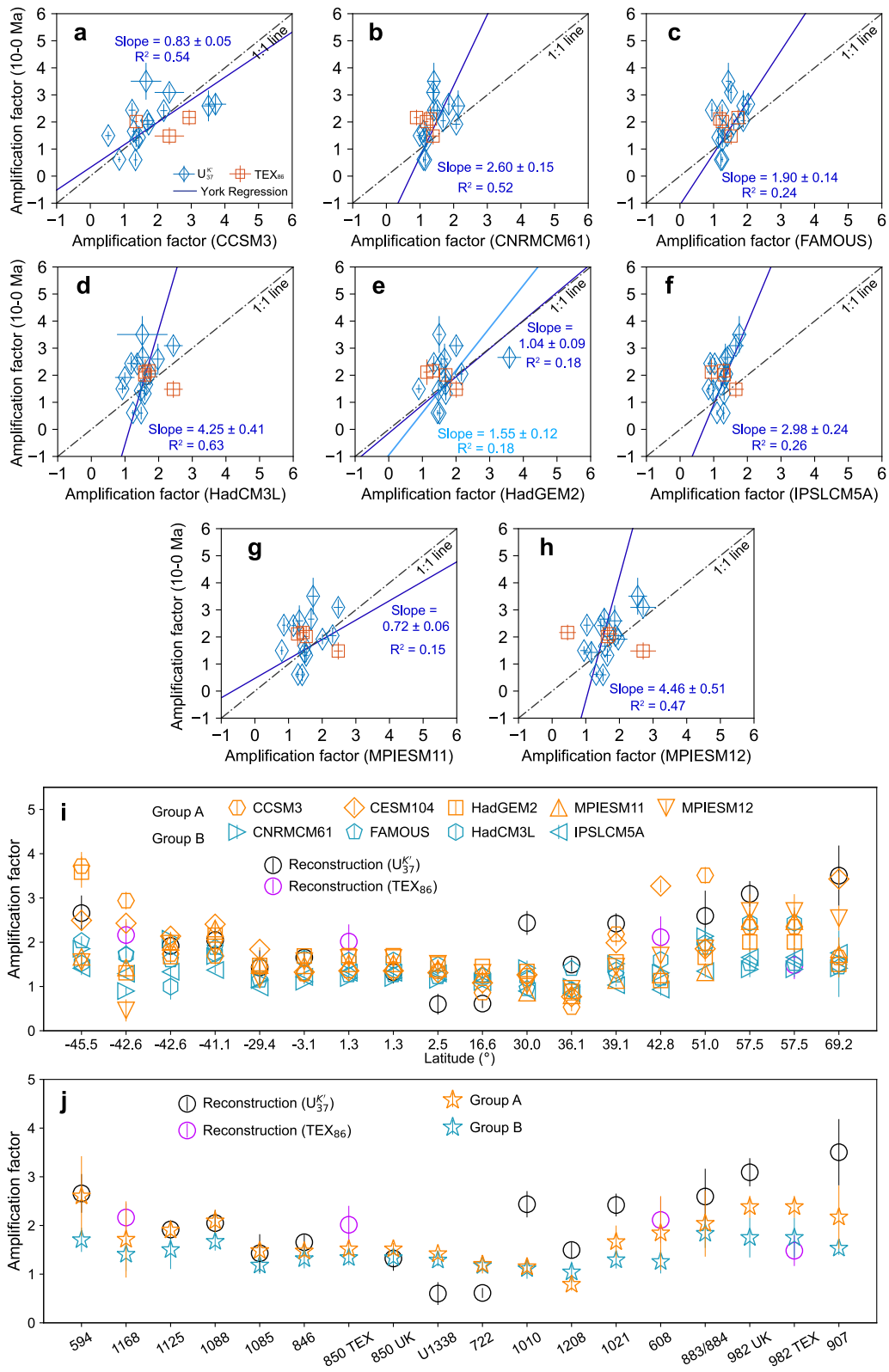

Figure 5.

To comprehensively assess the pattern similarity between paleo-results and multiple model simulations, we go beyond York Regression slopes and use a Taylor Diagram. This diagram incorporates various metrics, such as standard deviations (STD) of amplification factors, correlation coefficients, and root-mean-square differences (RMSD), to evaluate model performance (Figure S8 in Supporting Information S1). Due to the high RMSD values (>0.6), we use STD and correlation coefficients as supplementary criteria to York Regression slopes, which is our primary method for ranking these models (Figure S9 in Supporting Information S1). MPIESM12 ranks third in terms of STD similarity to the paleo-data, following CESM104 and CCSM3 (Figures S8 and S9 in Supporting Information S1). This, combined with York Regression results, allows us to group CESM104, CCSM3, HadGEM2, MPIESM11, and MPIESM12 into one category, Group A (Figure 5i), which demonstrate similar warming patterns to paleo-results (Figures 5a, 5e, and 5g and Figure S8 in Supporting Information S1). The remaining LongRunMIP models, including CNRM-CM6-1, FAMOUS, HadCM3L, and IPSL-CM5A, are categorized as Group B (Figure 5i), as their simulated warming patterns deviate from paleo-results (Figures 5b–5d and 5f and Figure S8 in Supporting Information S1, and Table S2 in Supporting Information S1). This classification provides a new framework for evaluating model performances in projecting future warming patterns, based on their ability to reproduce fundamental aspects of Earth's climate response observed in the geological record.

The comparison of multi-model mean of amplification factors between Group A and B shows stronger amplified warming in middle and high latitudes for Group A (Figure 5j). The larger high-latitude amplification factors in Group A (Text S8 and Figure S10 in Supporting Information S1) are unlikely due to the higher ECS, as not all Group A models have higher ECS than Group B models (Table S2 in Supporting Information S1). Also, analyses of CMIP5 and CMIP6 model outputs reveal no strong correlation between high latitude amplification and ECS (Text S9 and Figure S11 in Supporting Information S1), and this lack of dependency of high-latitude amplification on ECS is also suggested by Zhu et al. (2024), which shows that meridional temperature structure at the same global mean surface temperature level for the Eocene is similar across three CESM versions with different ECS values. Instead, Group A's stronger amplification likely stems from more effective positive feedback, such as surface albedo (Crook et al., 2011; Screen & Simmonds, 2010; Taylor et al., 2013), water vapor feedbacks, and cloud feedbacks (Taylor et al., 2013; Vavrus, 2004). This is supported by Group A's stronger shortwave clear-sky feedbacks and longwave cloud feedbacks at high latitudes (Text S10, Figures S12b and S12e in Supporting Information S1), despite counterbalancing effects from long-wave clear-sky feedbacks and shortwave cloud feedbacks (Figures S12c and S12d in Supporting Information S1). Other factors such as lapse rate feedback (Goosse et al., 2018; Pithan & Mauritsen, 2014; Stuecker et al., 2018) and atmospheric/ocean heat transport (Alexeev & Jackson, 2013; Goosse et al., 2018; Lu & Cai, 2010), might also contribute to inter-model differences in high-latitude amplification. However, evaluating their specific contribution using the radiative kernel technique is not feasible here due to the unavailability of essential feedback-associated variables (e.g., cloud profile) in the LongRunMIP outputs.

The "pattern effect" in modern climatology emphasizes the importance of zonal SST patterns across the tropical Pacific, particularly the differential warming between the western Pacific ascent regions and the eastern Pacific subsidence regions (Andrews & Webb, 2018; Dong et al., 2019; Zhou et al., 2017). While the spatial coverage of paleo-SST records in this study is limited compared to modern observations, our analysis provides key insights into the long-term evolution of these patterns. For example, the eastern equatorial Pacific is relatively well represented for establishing long-term SSTs, as indicated by Sites 846 (3.1°S, 90.8°W), 850 (1.5°N, 110.3°W), and U1338 (2.5°N, 118.0°W) in our analyses (Figure 3): the majority of the models capture the amplified

Figure 5. Comparing amplification factors between the last 10 million years geological data and model simulations from LongRunMIP. (a–h) show comparisons between data and model results obtained from CCSM3, CNRMCM61, FAMOUS, HadCM3L, HadGEM2, IPSLCM5A, MPIESM11, and MPIESM12, respectively. Diamonds and squares indicate amplification factors derived from $U_{37}^{K'}$ and TEX_{86}-based sea surface temperatures (SSTs), respectively, and blue lines indicate York Regression using all the data, while the light-blue line in (e) indicates York Regression excluding the rightmost data point (Site 594). In (a), the linear relationship between the SST of Site 608 and the Western Pacific Warm Pool SST from model outputs is not significant at 5% significance level, indicating the absence of the amplification factor for Site 608, and thus not shown in the plot. (i), Paleo-results versus model results of each site. Note that the *x*-axis in (i) and (j) are identical. In (i), the *x*-axis is represented by the latitude of the sites, while in (j), the sites names are displayed. Black and purple circles represent amplification factors based on $U_{37}^{K'}$-SST and TEX_{86}-SST, respectively. Orange symbols indicate models whose amplification factors are overall consistent with paleo-results, including CCSM3, CESM104, HadGEM2, MPIESM11, and MPIESM12 (Group A). Blue symbols indicate the rest of the models, including CNRM-CM6-1, FAMOUS, HadCM3L, and IPSL-CM5A (Group B). Error bars indicate two standard errors. (j), Comparisons between paleo-results and the multi-model mean of Group A and B. Orange and blue error bars indicate two standard errors of the ensemble mean.

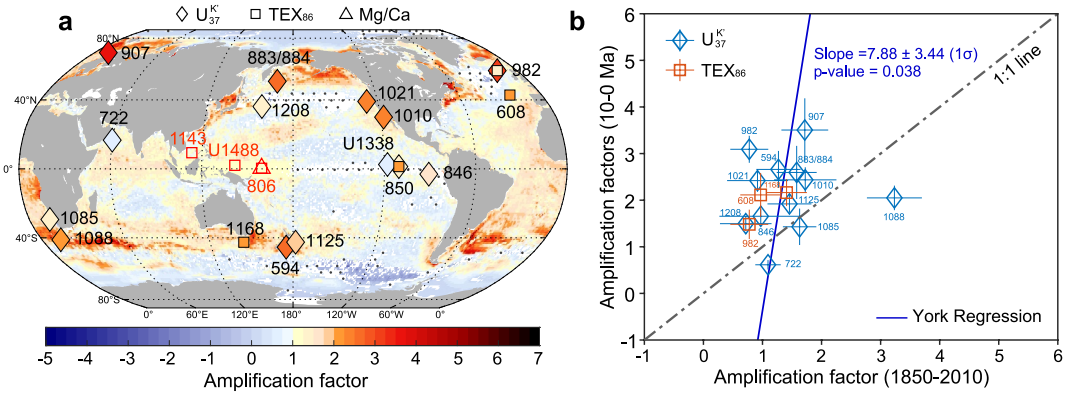

Figure 6. Comparing amplification factors between the last 10 million years (Myr) and the last 160 years. (a), The map shows the warming pattern of the global ocean. The color represents the amplification factors over a period of 160 years (1850–2010) derived from the HadISST2.1 data set. Stippling on the map indicate areas where the amplification factor is not available. This absence is due to the lack of a significant linear relationship between the sea surface temperature (SST) at a particular grid point and the Western Pacific Warm Pool (WPWP) SST, determined at a 5% significance level (Text S11 in Supporting Information S1). Filled diamonds and squares indicate 10-million-year amplification factors derived from $U_{37}^{K'}$-based and TEX_{86}-based SSTs, respectively. Red square and triangle symbols represent the WPWP sites used for producing the WPWP SST stack. (b), Comparing amplification factors between the recent 160 years and the past 10 Myr with a cross plot. Error bars indicate two standard errors. The gray dashed line represents the 1:1 line, and the blue line indicates York Regression with a slope of 7.88 ± 3.44 (1σ). For grid points closest to the paleo-locations of Sites 850 or 1338, the averaged SST from 1850 to 2010 does not exhibit a significant linear relationship with the WPWP SST (p-value > 0.05), and therefore data from Sites 850 and 1338 are not included in the cross plot (b).

warming derived from $U_{37}^{K'}$ proxy at Site 846 and/or 850 (Figure S13 in Supporting Information S1), suggesting that models reproduce the weakening of zonal SST gradients across the tropical Pacific under long-term warming. However, while the zonal gradient is reduced, it never completely disappears, maintaining the fundamental east-west temperature structure (Zhang et al., 2014). There is a discrepancy at Site U1338, where the amplified warming predicted by the models is not found in the proxy data (Figure 4), likely due to $U_{37}^{K'}$ values reaching their upper limit value for the late Miocene. The models' strong performance in reproducing long-term zonal SST gradient weakening contrasts with their poor performance in capturing the historically observed strengthening of these gradients (Heede & Fedorov, 2021; Seager et al., 2019; Wills et al., 2022), highlighting the importance of timescale in understanding tropical Pacific climate dynamics. Although the paleo-SST records cannot capture the complexity of modern pattern effects, our analysis of zonal warming patterns over extended timescales advances our understanding of Earth's climate system dynamics.

5. Comparing the Paleo-Warming Pattern With Recent Observations

Our approach of using paleo-SSTs to build long-term, equilibrium warming patterns of the ocean also provides an opportunity to assess their relationship with the observed ocean warming of the Common Era, which is yet to fully unfold. Popular SST data sets such as HadISST2.1, ERSSTv5, and COBE-SST2 which depict global ocean warming over the past 160 years, show slight deviations in the warming pattern (Figure 6a, Text S11, Figures S14a and S14c in Supporting Information S1) due to differences in the methods used for correcting historical SST biases (Kent et al., 2017; Smith & Reynolds, 2002). Nevertheless, all three SST data sets show that recent amplification factors are significantly lower than those over the past 10 Myr (Figure 6b, Figures S14b and S14d in Supporting Information S1). This contrast between modern and paleo-patterns offers crucial insights into future warming evolution: the modern pattern reflects a transient state influenced by ocean heat uptake, while the paleo-pattern represents the system's equilibrium response–essential for understanding long-term climate projections.

The Neogene records show larger amplification factors compared to those during the instrumental period (Figure 6 and Figure S14 in Supporting Information S1), especially at sites in the North Atlantic and Southern Ocean. This pattern is similar to the differences observed between equilibrium runs and transient 1–150 year runs simulated by some of the LongRunMIP models, such as CCSM3, CESM, MPIESM11, and MPIESM12, where

10.1029/2025AV001719

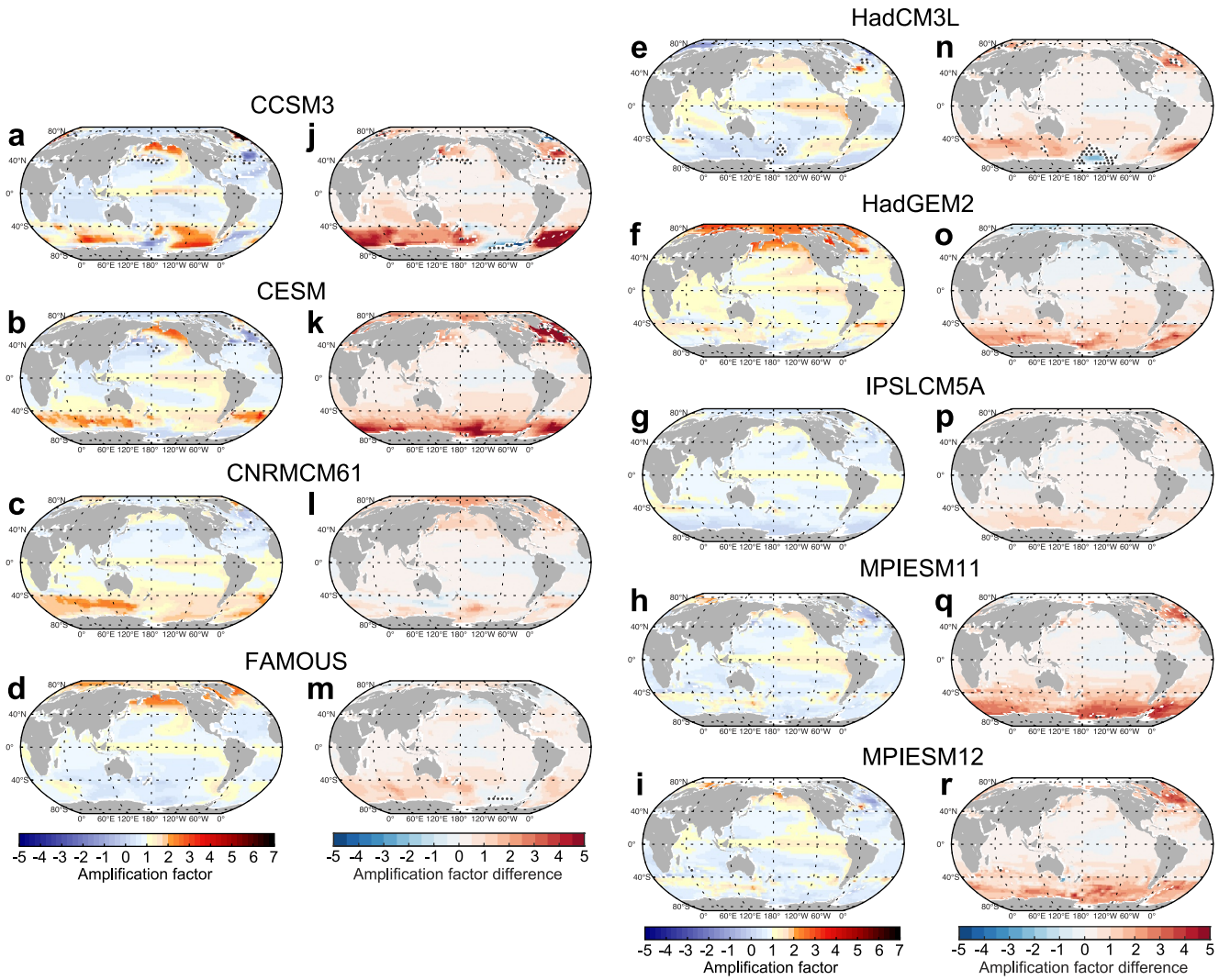

Figure 7. Comparing amplification factors between equilibrium and transient climate simulations obtained from LongRunMIP. (a–i) Show amplification factors estimated from transient 1–150 year runs generated by CCSM3, CESM, CNRMCM61, FAMOUS, HadCM3L, HadGEM2, IPSLCM5A, MPIESM11, and MPIESM12, respectively. (j–r) Show the differences from their corresponding equilibrium runs, which are displayed in Figures 3a and 4.

equilibrium runs also display larger amplification factors (Figure 7). These findings align with the stronger warming of these regions shown in equilibrium climate change simulations compared to the transient climate change simulations (Huang et al., 2020; King et al., 2020). The current reduced warming in the North Atlantic and Southern Ocean is likely due to deep-ocean heat uptake and changes in meridional overturning circulation (Jansen et al., 2018; Li et al., 2013). This suggests a temporary modulation, indicating additional warming in these regions as the climate system moves toward equilibrium. In addition, the observed pattern of warming over the last 160 years could be affected by internal modes of variability (Dessler, 2020), which are likely averaged out in the paleo-SST records.

Amplification factors can vary with warming levels (Figure S3f in Supporting Information S1), potentially explaining differences between the recent 160 years (~0.6°C WPWP warming) and the Neogene period (~4.5°C WPWP warming). However, our segmented analysis by warming levels reveals that the pattern of amplified warming remains largely consistent across different degrees of warming (Figure S3f in Supporting Information S1), indicating that the spatial pattern of amplification factors is relatively stable under diverse mean climate conditions.

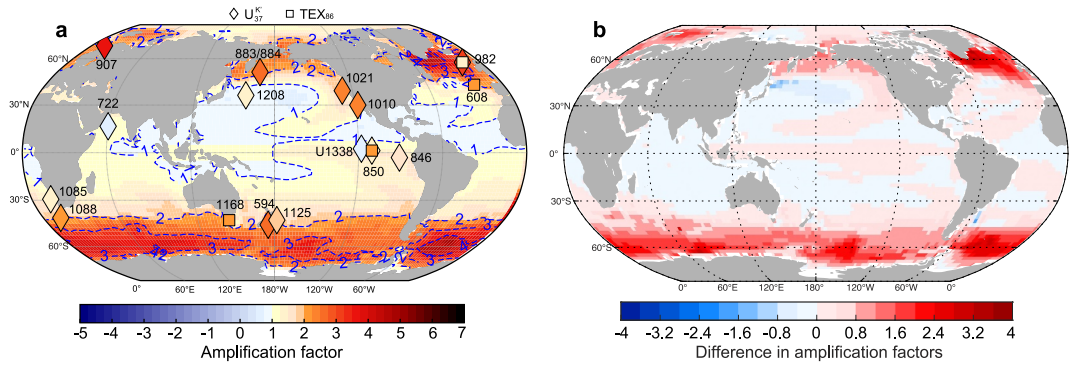

Figure 8. Future pattern of amplified warming relative to the Western Pacific Warm Pool (WPWP). (a), Equilibrium pattern of amplified warming relative to the WPWP. The colors show the multi-model mean of amplification factors derived from CESM, CCSM3, HadGEM2, MPIESM11, and MPIESM12. Blue dashed lines show the contour of amplification factors. Symbols are paleo-results identical to those shown in Figure 3a. (b), Differences between the equilibrium warming pattern (a) and predicted future warming pattern from 2101 to 2300 (Figure S15 in Supporting Information S1) that was based on a simulation from an extension of the SSP585 scenario for CMIP6.

6. Projecting the Future, Equilibrium Warming Pattern of the Global Ocean

The diverging warming patterns observed on different timescales imply that the future equilibrium warming pattern will display stronger amplified warming in middle and high latitudes compared to the current transient pattern, with significant implications for long-term adaptation in these regions. Given the similarity of Group A models (CESM, CCSM3, HadGEM2, MPIESM11, and MPIESM12) to the paleo-warming pattern, we utilize their ensemble mean equilibrium patterns to project future ocean warming (Figure 8a). Figure 8a shows the expected warming in different oceanic regions relative to a 1°C increase in WPWP surface temperature.

It is important to note that the timescale for reaching equilibrium in our projection is on the order of thousands of years, far beyond most policy-relevant climate projections. However, this long-term perspective offers valuable insights into the Earth's climate trajectory. Our projected equilibrium pattern (Figure 8b) shows a strong correlation (coefficient ~0.67) with projected warming patterns from 2101 to 2300 under a high CO_2 emission scenario (Figure S15 in Supporting Information S1), while revealing more pronounced high-latitude warming, particularly in the North Atlantic and Southern Ocean (Figure 8b). This discrepancy between equilibrium and century-scale projections underscores the importance of considering long-term climate evolution.

The expected transition from transient to equilibrium ocean surface warming patterns (Andrews et al., 2015; Dong et al., 2019; Gregory & Andrews, 2016; Sherwood et al., 2020; Wills et al., 2022) has a notable impact on the global radiative feedback changes (Dong et al., 2019), which in turn affects ECS (Sherwood et al., 2020). Previous work using relatively short (150-year) abrupt 4×CO_2 simulations (Zhou et al., 2021) showed that the pattern effect increases equilibrium committed warming by ~1°C. Our estimates of the pattern effect based on millennial timescale simulations show an even stronger pattern effect (Text S12 in Supporting Information S1, Table 1) than estimates from 150-year simulations (Andrews et al., 2022; Modak & Mauritsen, 2023), due to the climate feedback parameter λ increasing by 14%–59% from centennial to millennial time scales (Table 1). Consequently, the projected committed warming is likely stronger than previously estimated (Table 1). As demonstrated in LongRunMIP simulations, extending the run length from centennial to millennial timescales results in sustained high-latitude warming, increasing the high-latitude amplification factor, particularly for the North Atlantic and Southern Ocean (Figures S16, S17, and Text S13 in Supporting Information S1).

Our findings suggest that current observations and near-term projections might underestimate equilibrium warming in high-latitude regions. The alignment between paleo-data and leading climate models indicates that, given sufficient time, the Earth system may approach a warming pattern similar to that seen in the geological past. However, reaching such equilibrium states may take several millennia and follow a nonlinear trajectory. Future research comparing transient and equilibrium simulations with proxy records across different time periods could help better constrain the evolution of warming patterns, enhancing projections for policy-relevant timescales.

Table 1
Comparison of Pattern Effect Estimated From 150-Year Simulations and Millennial-Length Simulations Under Abrupt-4×CO_2

Model name	Historical climate feedback parameter (λ_{hist})	Feedback parameter derived from abrupt-4×CO_2 simulations ($\lambda_{4\times CO_2}$)		Pattern effect ($\Delta\lambda = \lambda_{4\times CO_2} - \lambda_{hist}$)	
		$\lambda_{4\times CO_2\_1\text{–}150}$	$\lambda_{4\times CO_2\_equilibrium}$	$\lambda_{4\times CO_2\_1\text{–}150} - \lambda_{hist}$	$\lambda_{4\times CO_2\_equilibrium} - \lambda_{hist}$
HadGEM2	−1.39	−0.63	−0.52	0.76	0.87
MPIESM11	−1.92	−1.36	−1.03	0.56	0.89
MPIESM12	−1.88	−1.39	−1.12	0.49	0.76

Note. λ_{hist} is calculated from Atmospheric Model Intercomparison Project (AMIP)-piForcing simulations of Andrews et al. (2022). $\lambda_{4\times CO_2}$ is calculated from climate simulations under an abrupt quadrupling of atmospheric CO_2 concentration (abrupt-4×CO_2). $\lambda_{4\times CO_2\_1\text{–}150}$ represents estimates based on the model outputs from 1 to 150 years and derived from Andrews et al. (2022). $\lambda_{4\times CO_2\_equilibrium}$ represents estimates based on the model outputs over the millennial-length simulations' final 15% of global mean warming (Rugenstein, Bloch-Johnson, Gregory, et al., 2020) and calculated by this study.

Conflict of Interest

The authors declare no conflicts of interest relevant to this study.

Data Availability Statement

The updated age model and sea surface temperatures for Sites 594 and 1125, the site-specific amplification factors estimated for the past 10 million years and from LongRunMIP models and recent observations, and the code used to bin paleotemperature records at selected time windows and overlaps are available at https://doi.org/10.6084/m9.figshare.24121185 (Liu et al., 2025). The SST outputs from CMIP5 and CMIP6 models were obtained from https://esgf-node.llnl.gov/search/cmip5/ and https://esgf-node.llnl.gov/search/cmip6/. The simulated Miocene SST output was obtained from https://doi.org/10.5281/zenodo.4568897 (Burls et al., 2021b).

Acknowledgments
We thank Dr. Andy Dessler for helpful discussions, Drs. Maria Rugenstein and Jonah Bloch-Johnson for providing LongRunMIP output. We thank all authors who have generated proxy-based SSTs for the past 10 million years and made them available. M.H. and X.L. were supported by National Science Foundation OCE-2217530 and OCE-2436683. Y.G.Z. was supported by the start-up grant from Guangzhou Institute of Geochemistry and the Chinese Academy of Sciences. Dr. Tim Herbert, two anonymous reviewers and Dr. Jess Tierney (Editor) are acknowledged for their insightful comments that help improve the quality of this article.

References

Alexeev, V. A., & Jackson, C. H. (2013). Polar amplification: Is atmospheric heat transport important? *Climate Dynamics*, *41*(2), 533–547. https://doi.org/10.1007/s00382-012-1601-z

Andrews, T., Bodas-Salcedo, A., Gregory, J. M., Dong, Y., Armour, K. C., Paynter, D., et al. (2022). On the effect of historical SST patterns on radiative feedback. *Journal of Geophysical Research: Atmospheres*, *127*(18), e2022JD036675. https://doi.org/10.1029/2022JD036675

Andrews, T., Gregory, J. M., & Webb, M. J. (2015). The dependence of radiative forcing and feedback on evolving patterns of surface temperature change in climate models. *Journal of Climate*, *28*(4), 1630–1648. https://doi.org/10.1175/jcli-d-14-00545.1

Andrews, T., & Webb, M. J. (2018). The dependence of global cloud and lapse rate feedbacks on the spatial structure of tropical Pacific warming. *Journal of Climate*, *31*(2), 641–654. https://doi.org/10.1175/JCLI-D-17-0087.1

Armour, K. C., Bitz, C. M., & Roe, G. H. (2013). Time-varying climate sensitivity from regional feedbacks. *Journal of Climate*, *26*(13), 4518–4534. https://doi.org/10.1175/JCLI-D-12-00544.1

Backman, J., Baldauf, J. G., Ciummelli, M., & Raffi, I. (2016). *Data report: A revised biomagnetostratigraphic age model for site U1338, IODP expedition 320/321*. Integrated Ocean Drilling Program Management International, Inc. https://doi.org/10.2204/iodp.proc.320321.219.2016

Blaauw, M., & Christen, J. A. (2011). Flexible paleoclimate age-depth models using an autoregressive gamma process. *Bayesian Analysis*, *6*(3), 457–474. https://doi.org/10.1214/11-BA618

Brierley, C. M., & Fedorov, A. V. (2016). Comparing the impacts of Miocene–Pliocene changes in inter-ocean gateways on climate: Central American Seaway, Bering Strait, and Indonesia. *Earth and Planetary Science Letters*, *444*, 116–130. https://doi.org/10.1016/j.epsl.2016.03.010

Burls, N. J., Bradshaw, C. D., De Boer, A. M., Herold, N., Huber, M., Pound, M., et al. (2021a). Simulating Miocene warmth: Insights from an opportunistic multi-model ensemble (MioMIP1). *Paleoceanography and Paleoclimatology*, *36*(5), e2020PA004054. https://doi.org/10.1029/2020PA004054

Burls, N. J., Bradshaw, C. D., De Boer, A. M., Herold, N., Huber, M., Pound, M., et al. (2021b). Simulating Miocene warmth: Insights from an opportunistic multi-model ensemble (MioMIP1) [Dataset]. *Zenodo*, *36*(5), e2020PA004054. https://doi.org/10.1029/2020pa004054

Caballero-Gill, R. P., Herbert, T. D., & Dowsett, H. J. (2019). 100-kyr paced climate change in the Pliocene warm period, Southwest Pacific. *Paleoceanography and Paleoclimatology*, *34*(4), 524–545. https://doi.org/10.1029/2018PA003496

Cleveland Stout, R., Proistosescu, C., & Roe, G. (2023). Fingerprinting low-frequency last millennium temperature variability in forced and unforced climate models. *Journal of Climate*, *36*(20), 7005–7023. https://doi.org/10.1175/JCLI-D-22-0810.1

Crook, J. A., Forster, P. M., & Stuber, N. (2011). Spatial patterns of modeled climate feedback and contributions to temperature response and polar amplification. *Journal of Climate*, *24*(14), 3575–3592. https://doi.org/10.1175/2011jcli3863.1

Dessler, A. E. (2020). Potential problems measuring climate sensitivity from the historical record. *Journal of Climate*, *33*(6), 2237–2248. https://doi.org/10.1175/JCLI-D-19-0476.1

Dong, Y., Armour, K. C., Zelinka, M. D., Proistosescu, C., Battisti, D. S., Zhou, C., & Andrews, T. (2020). Intermodel spread in the pattern effect and its contribution to climate sensitivity in CMIP5 and CMIP6 models. *Journal of Climate*, *33*(18), 7755–7775. https://doi.org/10.1175/JCLI-D-19-1011.1

Dong, Y., Proistosescu, C., Armour, K. C., & Battisti, D. S. (2019). Attributing historical and future evolution of radiative feedbacks to regional warming patterns using a Green? function approach: The preeminence of the Western Pacific. *Journal of Climate*, *32*(17), 5471–5491. https://doi.org/10.1175/JCLI-D-18-0843.1

Forster, P., Storelvmo, T., Armour, K., Collins, W., Dufresne, J.-L., Frame, D., et al. (2021). The Earth's energy budget, climate feedbacks, and climate sensitivity. In V. Masson-Delmotte, P. Zhai, A. Pirani, S. L. Connors, C. Péan, S. Berger, et al. (Eds.), *Climate change 2021: The physical science basis. Contribution of Working Group I to the sixth assessment report of the intergovernmental Panel on climate change*. Cambridge University Press. https://doi.org/10.1017/9781009157896.009

Franke, J. G., Werner, J. P., & Donner, R. V. (2017). Reconstructing Late Holocene North Atlantic atmospheric circulation changes using functional paleoclimate networks. *Climate of the Past*, *13*(11), 1593–1608. https://doi.org/10.5194/cp-13-1593-2017

Fu, R., Genio, A. D. D., & Rossow, W. B. (1994). Influence of ocean surface conditions on atmospheric vertical thermodynamic structure and deep convection. *Journal of Climate*, *7*(7), 1092–1108. https://doi.org/10.1175/1520-0442(1994)007<1092:IOOSCO>2.0.CO;2

Fueglistaler, S. (2019). Observational evidence for two modes of coupling between sea surface temperatures, tropospheric temperature profile, and shortwave cloud radiative effect in the tropics. *Geophysical Research Letters*, *46*(16), 9890–9898. https://doi.org/10.1029/2019GL083990

Gebbie, G., & Huybers, P. (2019). The little ice age and 20th-century deep Pacific cooling. *Science*, *363*(6422), 70–74. https://doi.org/10.1126/science.aar8413

Goosse, H., Kay, J. E., Armour, K. C., Bodas-Salcedo, A., Chepfer, H., Docquier, D., et al. (2018). Quantifying climate feedbacks in polar regions. *Nature Communications*, *9*(1), 1919. https://doi.org/10.1038/s41467-018-04173-0

Gradstein, F. M., Ogg, J. G., Schmitz, M., & Ogg, G. (2012). *The Geologic time scale 2012 2-volume set*. Elsevier.

Gregory, J. M., & Andrews, T. (2016). Variation in climate sensitivity and feedback parameters during the historical period. *Geophysical Research Letters*, *43*(8), 3911–3920. https://doi.org/10.1002/2016GL068406

Heede, U. K., & Fedorov, A. V. (2021). Eastern equatorial Pacific warming delayed by aerosols and thermostat response to CO_2 increase. *Nature Climate Change*, *11*(8), 696–703. https://doi.org/10.1038/s41558-021-01101-x

Herbert, T. D., Lawrence, K. T., Tzanova, A., Peterson, L. C., Caballero-Gill, R., & Kelly, C. S. (2016). Late Miocene global cooling and the rise of modern ecosystems. *Nature Geoscience*, *9*(11), 843–847. https://doi.org/10.1038/ngeo2813

Huang, D., Dai, A., & Zhu, J. (2020). Are the transient and equilibrium climate change patterns similar in response to increased CO_2? *Journal of Climate*, *33*(18), 8003–8023. https://doi.org/10.1175/JCLI-D-19-0749.1

Jansen, M. F., Nadeau, L.-P., & Merlis, T. M. (2018). Transient versus equilibrium response of the ocean's overturning circulation to warming. *Journal of Climate*, *31*(13), 5147–5163. https://doi.org/10.1175/JCLI-D-17-0797.1

Kent, E. C., Kennedy, J. J., Smith, T. M., Hirahara, S., Huang, B., Kaplan, A., et al. (2017). A call for new approaches to quantifying biases in observations of sea surface temperature. *Bulletin of the American Meteorological Society*, *98*(8), 1601–1616. https://doi.org/10.1175/BAMS-D-15-00251.1

King, A. D., Lane, T. P., Henley, B. J., & Brown, J. R. (2020). Global and regional impacts differ between transient and equilibrium warmer worlds. *Nature Climate Change*, *10*(1), 42–47. https://doi.org/10.1038/s41558-019-0658-7

Lawrence, K. T., Coxall, H. K., Sosdian, S. M., & Steinthorsdottir, M. (2021). Navigating Miocene ocean temperatures for insights into the future. *Eos*, *102*. https://doi.org/10.1029/2021EO210528

Lewis, N., & Mauritsen, T. (2021). Negligible unforced historical pattern effect on climate feedback strength found in HadISST-Based AMIP simulations. *Journal of Climate*, *34*(1), 39–55. https://doi.org/10.1175/JCLI-D-19-0941.1

Li, C., von Storch, J.-S., & Marotzke, J. (2013). Deep-ocean heat uptake and equilibrium climate response. *Climate Dynamics*, *40*(5), 1071–1086. https://doi.org/10.1007/s00382-012-1350-z

Liu, X., Herold, N., & Huber, M. (2024). Atlantic meridional overturning circulation influence on the annual mean intertropical convergence zone location in the Miocene. *Geophysical Research Letters*, *51*(9), e2024GL109159. https://doi.org/10.1029/2024GL109159

Liu, X., Huber, M., Foster, G. L., Dessler, A., & Zhang, Y. G. (2022). Persistent high latitude amplification of the Pacific Ocean over the past 10 million years. *Nature Communications*, *13*(1), 7310. https://doi.org/10.1038/s41467-022-35011-z

Liu, X., Zhang, Y. G., Huber, M., Chang, P., & Wang, L. (2025). Connecting warming patterns of the paleo-ocean to our future [Dataset]. *figshare*. https://doi.org/10.6084/m9.figshare.24121185

Locarnini, M., Mishonov, A., Baranova, O., Boyer, T., Zweng, M., Garcia, H., et al. (2018). World ocean atlas 2018, volume 1: Temperature. In *NOAA Atlas NESDIS 73 (Sydney Levitus)*. National Environmental Satellite, Data, and Information Service.

Lu, J., & Cai, M. (2010). Quantifying contributions to polar warming amplification in an idealized coupled general circulation model. *Climate Dynamics*, *34*(5), 669–687. https://doi.org/10.1007/s00382-009-0673-x

Modak, A., & Mauritsen, T. (2023). Better-constrained climate sensitivity when accounting for dataset dependency on pattern effect estimates. *Atmospheric Chemistry and Physics*, *23*(13), 7535–7549. https://doi.org/10.5194/acp-23-7535-2023

Otto-Bliesner, B. L., Jahn, A., Feng, R., Brady, E. C., Hu, A., & Löfverström, M. (2017). Amplified North Atlantic warming in the late Pliocene by changes in Arctic gateways. *Geophysical Research Letters*, *44*(2), 957–964. https://doi.org/10.1002/2016GL071805

Pithan, F., & Mauritsen, T. (2014). Arctic amplification dominated by temperature feedbacks in contemporary climate models. *Nature Geoscience*, *7*(3), 181–184. https://doi.org/10.1038/ngeo2071

Rugenstein, M., Bloch-Johnson, J., Abe-Ouchi, A., Andrews, T., Beyerle, U., Cao, L., et al. (2020). LongRunMIP: Motivation and design for a large collection of millennial-length AOGCM simulations. *Bulletin of the American Meteorological Society*, *100*(12), 2551–2570. https://doi.org/10.1175/bams-d-19-0068.1

Rugenstein, M., Bloch-Johnson, J., Gregory, J., Andrews, T., Mauritsen, T., Li, C., et al. (2020). Equilibrium climate sensitivity estimated by equilibrating climate models. *Geophysical Research Letters*, *47*(4), e2019GL083898. https://doi.org/10.1029/2019GL083898

Screen, J. A., & Simmonds, I. (2010). The central role of diminishing sea ice in recent Arctic temperature amplification. *Nature*, *464*(7293), 1334–1337. https://doi.org/10.1038/nature09051

Seager, R., Cane, M., Henderson, N., Lee, D.-E., Abernathey, R., & Zhang, H. (2019). Strengthening tropical Pacific zonal sea surface temperature gradient consistent with rising greenhouse gases. *Nature Climate Change*, *9*(7), 517–522. https://doi.org/10.1038/s41558-019-0505-x

Sherwood, S. C., Webb, M. J., Annan, J. D., Armour, K. C., Forster, P. M., Hargreaves, J. C., et al. (2020). An assessment of Earth's climate sensitivity using multiple lines of evidence. *Reviews of Geophysics*, *58*(4), e2019RG000678. https://doi.org/10.1029/2019RG000678

Smith, T. M., & Reynolds, R. W. (2002). Bias corrections for historical sea surface temperatures based on marine air temperatures. *Journal of Climate*, *15*(1), 73–87. https://doi.org/10.1175/1520-0442(2002)015<0073:BCFHSS>2.0.CO;2

Stuecker, M. F., Bitz, C. M., Armour, K. C., Proistosescu, C., Kang, S. M., Xie, S.-P., et al. (2018). Polar amplification dominated by local forcing and feedbacks. *Nature Climate Change*, *8*(12), 1076–1081. https://doi.org/10.1038/s41558-018-0339-y

Sud, Y. C., Walker, G. K., Zhou, Y. P., Schmidt, G. A., Lau, K.-M., & Cahalan, R. F. (2008). Effects of doubled CO_2 on tropical sea surface temperatures (SSTs) for onset of deep convection and maximum SST: Simulations based inferences. *Geophysical Research Letters*, *35*(12), L12707. https://doi.org/10.1029/2008GL033872

Taylor, P. C., Cai, M., Hu, A., Meehl, J., Washington, W., & Zhang, G. J. (2013). A decomposition of feedback contributions to polar warming amplification. *Journal of Climate*, *26*(18), 7023–7043. https://doi.org/10.1175/JCLI-D-12-00696.1

Tierney, J. E., King, J., Osman, M. B., Abell, J. T., Burls, N. J., Erfani, E., et al. (2025). Pliocene warmth and patterns of climate change inferred from paleoclimate data assimilation. *AGU Advances*, *6*(1), e2024AV001356. https://doi.org/10.1029/2024AV001356

Tierney, J. E., & Tingley, M. P. (2014). A Bayesian, spatially-varying calibration model for the TEX 86 proxy. *Geochimica et Cosmochimica Acta*, *127*, 83–106. https://doi.org/10.1016/j.gca.2013.11.026

Tierney, J. E., & Tingley, M. P. (2018). BAYSPLINE: A new calibration for the alkenone paleothermometer. *Paleoceanography and Paleoclimatology*, *33*(3), 281–301. https://doi.org/10.1002/2017pa003201

Tierney, J. E., Zhu, J., King, J., Malevich, S. B., Hakim, G. J., & Poulsen, C. J. (2020). Glacial cooling and climate sensitivity revisited. *Nature*, *584*(7822), 569–573. https://doi.org/10.1038/s41586-020-2617-x

Tierney, J. E., Zhu, J., Li, M., Ridgwell, A., Hakim, G. J., Poulsen, C. J., et al. (2022). Spatial patterns of climate change across the Paleocene–Eocene Thermal maximum. *Proceedings of the National Academy of Sciences*, *119*(42), e2205326119. https://doi.org/10.1073/pnas.2205326119

Vavrus, S. (2004). The impact of cloud feedbacks on Arctic climate under greenhouse forcing. *Journal of Climate*, *17*(3), 603–615. https://doi.org/10.1175/1520-0442(2004)017<0603:TIOCFO>2.0.CO;2

Williams, I. N., Pierrehumbert, R. T., & Huber, M. (2009). Global warming, convective threshold and false thermostats. *Geophysical Research Letters*, *36*(21), L21805. https://doi.org/10.1029/2009gl039849

Wills, R. C. J., Dong, Y., Proistosecu, C., Armour, K. C., & Battisti, D. S. (2022). Systematic climate model biases in the large-scale patterns of recent sea-surface temperature and sea-level pressure change. *Geophysical Research Letters*, *49*(17), e2022GL100011. https://doi.org/10.1029/2022GL100011

York, D., Evensen, N. M., Martínez, M. L., & De Basabe Delgado, J. (2004). Unified equations for the slope, intercept, and standard errors of the best straight line. *American Journal of Physics*, *72*(3), 367–375. https://doi.org/10.1119/1.1632486

Zhang, Y. G., Pagani, M., & Liu, Z. (2014). A 12-million-year temperature history of the tropical Pacific Ocean. *Science*, *344*(6179), 84–87. https://doi.org/10.1126/science.1246172

Zhou, C., Zelinka, M. D., Dessler, A. E., & Wang, M. (2021). Greater committed warming after accounting for the pattern effect. *Nature Climate Change*, *11*(2), 132–136. https://doi.org/10.1038/s41558-020-00955-x

Zhou, C., Zelinka, M. D., & Klein, S. A. (2017). Analyzing the dependence of global cloud feedback on the spatial pattern of sea surface temperature change with a Green's function approach. *Journal of Advances in Modeling Earth Systems*, *9*(5), 2174–2189. https://doi.org/10.1002/2017MS001096

Zhu, J., Poulsen, C. J., & Otto-Bliesner, B. L. (2024). Modeling past hothouse climates as a means for assessing earth system models and improving the understanding of warm climates. *Annual Review of Earth and Planetary Sciences*, *52*(1), 351–378. https://doi.org/10.1146/annurev-earth-032320-100333

References From the Supporting Information

Beltran, C., Rousselle, G., de Rafélis, M., Sicre, M.-A., Labourdette, N., & Schouten, S. (2019). Evolution of the zonal gradients across the equatorial Pacific during the Miocene–Pleistocene. *Journal of Sedimentary Research*, *89*(3), 242–252. https://doi.org/10.2110/jsr.2019.15

Cao, X., Zahirovic, S., Li, S., Suo, Y., Wang, P., Liu, J., & Müller, R. D. (2020). A deforming plate tectonic model of the South China Block since the Jurassic. *Gondwana Research*, *102*, 3–16. https://doi.org/10.1016/j.gr.2020.11.010

Chiswell, S. M. (2002). Temperature and salinity mean and variability within the subtropical front over the Chatham rise, New Zealand. *New Zealand Journal of Marine & Freshwater Research*, *36*(2), 281–298. https://doi.org/10.1080/00288330.2002.9517086

Herbert, T. D., Lawrence, K. T., Tzanova, A., Peterson, L. C., Caballero-Gill, R. P., & Kelly, C. S. (2018a). (Table S2) SST estimates as a function of age, ODP Site 151-907. *PANGAEA*. https://doi.org/10.1594/PANGAEA.885594

Herbert, T. D., Lawrence, K. T., Tzanova, A., Peterson, L. C., Caballero-Gill, R. P., & Kelly, C. S. (2018b). (Table S2) SST estimates as a function of age, ODP Site 162-982. *PANGAEA*. https://doi.org/10.1594/PANGAEA.885578

Hirahara, S., Ishii, M., & Fukuda, Y. (2014). Centennial-scale sea surface temperature analysis and its uncertainty. *Journal of Climate*, *27*(1), 57–75. https://doi.org/10.1175/JCLI-D-12-00837.1

Hou, S., Lamprou, F., Hoem, F. S., Hadju, M. R. N., Sangiorgi, F., Peterse, F., & Bijl, P. K. (2023). Lipid-biomarker-based sea surface temperature record offshore Tasmania over the last 23 million years. *Climate of the Past*, *19*(4), 787–802. https://doi.org/10.5194/cp-19-787-2023

Huang, B., Thorne, P. W., Banzon, V. F., Boyer, T., Chepurin, G., Lawrimore, J. H., et al. (2017). *NOAA extended reconstructed sea surface temperature (ERSST), version 5*. NOAA National Centers for Environmental Information.

Jones, C., Liddicoat, S., & Wiltshire, A. (2021). MOHC UKESM1.0-LL model output prepared for CMIP6 CDRMIP esm-ssp585ext [Dataset]. *Earth System Grid Federation*. https://doi.org/10.22033/ESGF/CMIP6.12211

Long, A., & Rippeteau, B. (1974). Testing contemporaneity and averaging radiocarbon dates. *American Antiquity*, *39*(2Part1), 205–215. https://doi.org/10.2307/279583

Müller, R. D., Zahirovic, S., Williams, S. E., Cannon, J., Seton, M., Bower, D. J., et al. (2019). A global plate model including lithospheric deformation along major rifts and orogens since the Triassic. *Tectonics*, *38*(6), 1884–1907. https://doi.org/10.1029/2018TC005462

O'Brien, C. L., Foster, G. L., Martínez-Botí, M. A., Abell, R., Rae, J. W., & Pancost, R. D. (2014). High sea surface temperatures in tropical warm pools during the Pliocene. *Nature Geoscience*, *7*(8), 606–611. https://doi.org/10.1038/ngeo2194

Rousselle, G., Beltran, C., Sicre, M.-A., Raffi, I., & De Rafélis, M. (2013). Changes in sea-surface conditions in the Equatorial Pacific during the middle Miocene–Pliocene as inferred from coccolith geochemistry. *Earth and Planetary Science Letters*, *361*, 412–421. https://doi.org/10.1016/j.epsl.2012.11.003

Super, J. R., Thomas, E., Pagani, M., Huber, M., O'Brien, C. L., & Hull, P. M. (2020). Miocene evolution of North Atlantic Sea surface temperature. *Paleoceanography and Paleoclimatology*, *35*(5), e2019PA003748. https://doi.org/10.1029/2019PA003748

Titchner, H. A., & Rayner, N. A. (2014). The Met Office Hadley Centre sea ice and sea surface temperature data set, version 2: 1. Sea ice concentrations. *Journal of Geophysical Research: Atmospheres*, *119*(6), 2864–2889. https://doi.org/10.1002/2013JD020316

Wara, M. W., Ravelo, A. C., & Delaney, M. L. (2005). Permanent El Niño-like conditions during the Pliocene warm period. *Science*, *309*(5735), 758–761. https://doi.org/10.1126/science.1112596

Young, A., Flament, N., Maloney, K., Williams, S., Matthews, K., Zahirovic, S., & Müller, R. D. (2019). Global kinematics of tectonic plates and subduction zones since the late Paleozoic Era. *Special Issue: Advances in Himalayan Tectonics*, *10*(3), 989–1013. https://doi.org/10.1016/j.gsf.2018.05.011

Zelinka, M. D., Myers, T. A., McCoy, D. T., Po-Chedley, S., Caldwell, P. M., Ceppi, P., et al. (2020). Causes of higher climate sensitivity in CMIP6 models. *Geophysical Research Letters*, *47*(1), e2019GL085782. https://doi.org/10.1029/2019GL085782